Accepted Manuscript

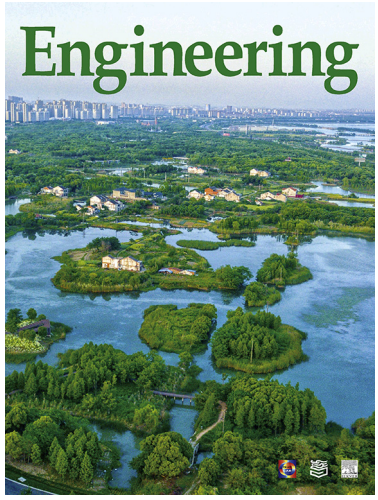

Article

Testing of a Full-Scale Composite Floor Plate

Dennis Lam, Xianghe Dai, Therese Sheehan

PII: S2095-8099(18)30723-9
DOI: https://doi.org/10.1016/j.eng.2018.11.021
Reference: ENG 174

To appear in: *Engineering*

Received Date: 25 July 2018
Revised Date: 15 September 2018
Accepted Date: 12 November 2018

Please cite this article as: D. Lam, X. Dai, T. Sheehan, Testing of a Full-Scale Composite Floor Plate, *Engineering* (2019), doi: https://doi.org/10.1016/j.eng.2018.11.021

Engineering 5 (2019) xxx-xxx

Research
High Performance Structures: Building Structures and Materials—Article

Testing of a Full-Scale Composite Floor Plate

Dennis Lam *, Xianghe Dai, Therese Sheehan
School of Engineering, University of Bradford, Bradford, United Kingdom

* Corresponding author.
E-mail address: d.lam1@bradford.ac.uk

RTICLE INFO
Article history:
Received 15 July 2018
Revised 16 September 2018
Accepted 11 November 2018
Available online

Keywords:
Floor plate test
Composite beams
Edge beams
Eurocode 4
In-plane effect
Column removal
Robustness

ABSTRACT
A full-scale composite floor plate was tested to investigate the flexural behavior and in-plane effects of the floor slab in a grillage of composite beams that reduces the tendency for longitudinal splitting of the concrete slab along the line of the primary beams. This is important in cases where the steel decking is discontinuous when it is orientated parallel to the beams. In this case, it is important to demonstrate that the amount of transverse reinforcement required to transfer local forces from the shear connectors can be reduced relative to the requirements of Eurocode 4. The mechanism under study involved in-plane compression forces being developed in the slab due to the restraining action of the floor plate, which was held in position by the peripheral composite beams; while the secondary beams acted as transverse ties to resist the forces in the floor plate that would otherwise lead to splitting of the slab along the line of the primary beams. The tendency for cracking along the center line of the primary beam and at the peripheral beams was closely monitored. This is the first large floor plate test that has been carried out under laboratory conditions since the Cardington tests in the early 1990s, although those tests were not carried out to failure. This floor plate test was designed so that the longitudinal force transferred by the primary beams was relatively high (i.e., it was designed for full shear connection), but the transverse reinforcement was taken as the minimum of 0.2% of the concrete area. The test confirmed that the primary beams reached their plastic bending resistance despite the discontinuous decking and transverse reinforcement at the minimum percentage given in Eurocode 4. Based on this test, a reduction factor due to shear connectors at edge beams without U-bars is proposed.

1. Introduction

Steel-concrete composite structures are the most common forms of flooring system used in steel-framed structures and have been widely used for many years all over the world [1–6]. Composite action generated between the steel beams and concrete slabs through the use of shear connectors could increase the load-bearing capacity and stiffness of the composite beams, which would lead to a significant saving in steel weight and construction cost.

The composite floor plate test presented in this paper investigated how the in-plane or membrane effects of the composite floor slab reduce the tendency for longitudinal splitting of the concrete slab along the line of the primary beams, and therefore increases the load capacity of the structural system. The floor plate test consisted of a grillage of primary beams, secondary beams, and columns. A series of tests was conducted. The first test was carried out with two-point loads applied to each of the internal secondary beams so that the primary beams were loaded via the secondary beams, as would be the case in practice. This test was repeated over a few cycles of working load and factored load, followed by an increase up to a load; this resulted in an acceptable maximum deflection that would not cause serious damage to the floor plate, which might affect subsequent tests. The second test series that was carried out focused on the edge beams by applying load directly onto these beams; this investigated the tendency for splitting of the concrete slab near its edge. On one edge, U-bars were used to provide local anchorage, whereas on the other edge, no additional reinforcement other than the mesh was used. Finally, a robustness test was performed on the side of the secondary edge beams without U-bars in which the support to the column was removed.

2. Details of the full-scale composite floor plate

2.1. Design of the composite floor plate

The dimensions of the composite floor plate were chosen to be 10.6 m long × 4.0 m wide, since these dimensions have the correct aspect ratio and easily fit in our laboratory. The composite floor plate consisted of nine beams (three primary beams and six secondary beams) and six columns, as shown in Fig. 1. All the primary beams (one central primary beam and two edge primary beams) were IPE270 in S355 steel and spanned 3.6 m between the flanges of the two columns. The two internal secondary beams were IPE300, also in S355 steel, and spanned 5.2 m between their connections to the web of the supporting beams. The other four edge secondary beams were IPE270 in S355 steel with a span of 5.2 m. The central primary beam (IPE 270) was designed to be 10% weaker than the internal secondary beams (IPE300) so that failure would occur first in the central primary beam.

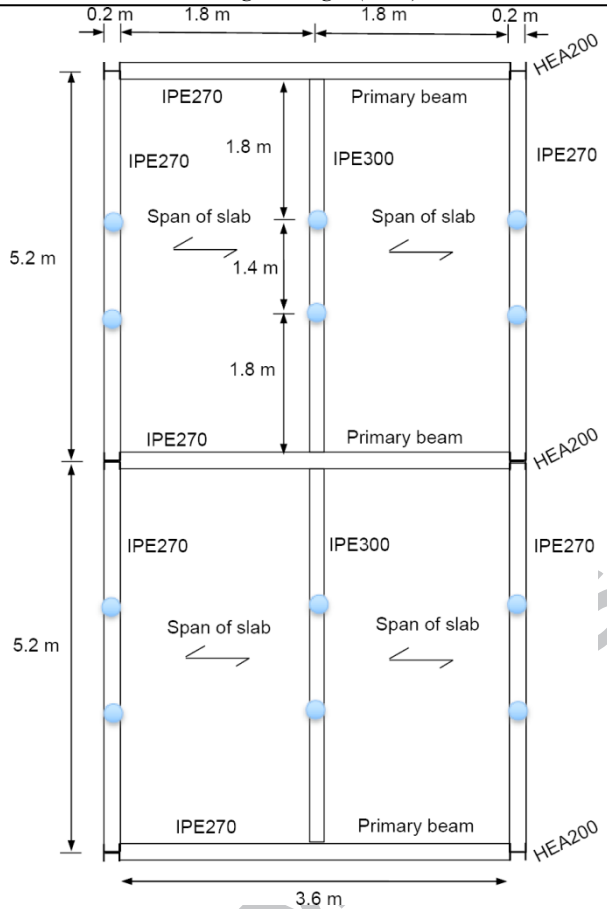

Fig. 1. Beam arrangement and floor plate dimensions. The blue spots represent the point load applied to the internal beam (test 1) and the external beam (test 2). The load cells were placed under the central columns.

2.2. Composite frame setup

The floor beams and columns arrangement are shown in Fig. 2. The columns were 1.0 m high and the two central columns were designed to be 200 mm shorter than the other four corner columns, so that load cells could be placed underneath them to monitor the loads transferred to the central columns. The two central columns were tied to prevent outward movement, since it is possible that a small moment might be generated in the columns through the connections. An endplate with the dimensions 180 mm × 220 mm × 10 mm was welded to the web of the internal secondary beams (IPE300, sections were notched to fit) and bolted to the web of the primary beams (IPE270) using six No. M20 Grade 8.8 bolts (the bolt spacing was 70 mm in the vertical direction and 100 mm in the horizontal direction). An endplate with the dimensions 140 mm × 220 mm × 10 mm was welded to the web of the secondary edge beams (IPE270) and bolted to the web of the HEA200 columns using six No. M20 Grade 8.8 bolts (the bolt spacing was 70 mm in both the horizontal and vertical directions). An endplate with the dimensions 170 mm × 220 mm × 10 mm was welded to the web of the primary beams (IPE270) and bolted to the flange of the HEA200 column using six No. M20 Grade 8.8 bolts (the bolt spacing was 70

mm in the vertical direction and 90 mm in the horizontal direction). Fig. 3 shows details of the beam-to-beam and beam-to-column connections.

Fig. 2. Layout of the beams and columns in the floor plate test.

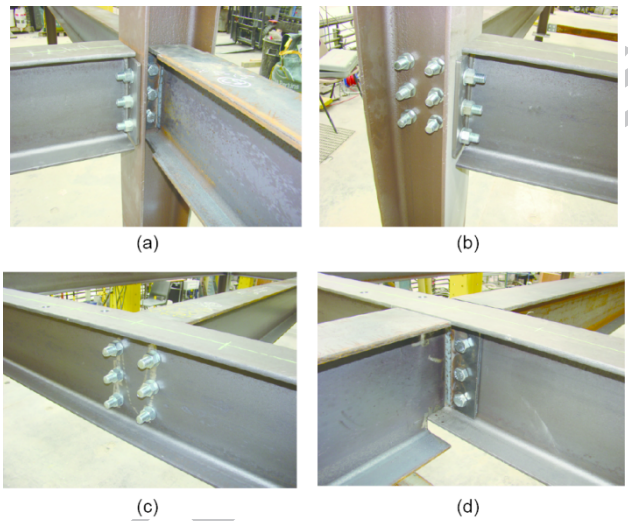

Fig. 3. Details of beam-to-beam and beam-to-column joints. (a) Central column connections; (b) corner column connections; (c) primary edge beam connections; (d) primary central beam connections.

2.3. Details of composite slab and shear connectors

The composite slabs consisted of a 130 mm thick slab with a 0.9 mm thick, 58 mm deep profiled decking (Cofraplus 60 from ArcelorMittal S.A.). The deck profile had ribs spaced at 207 mm and allowed the welding of a stud in the middle of the rib. Single 19 mm diameter shear studs (100 mm nominal height) were used, and the spacing of the studs was chosen to be 200 mm for the primary internal beams and 207 mm for all the secondary beams. Since the profiled decking was discontinued at the primary beam, the shear connectors were welded directly to the primary beams while through deck welding was used for the secondary beams. The shear connector details are shown in Figs. 4 and 5.

Fig. 4. Steel decking and shear connector arrangement.

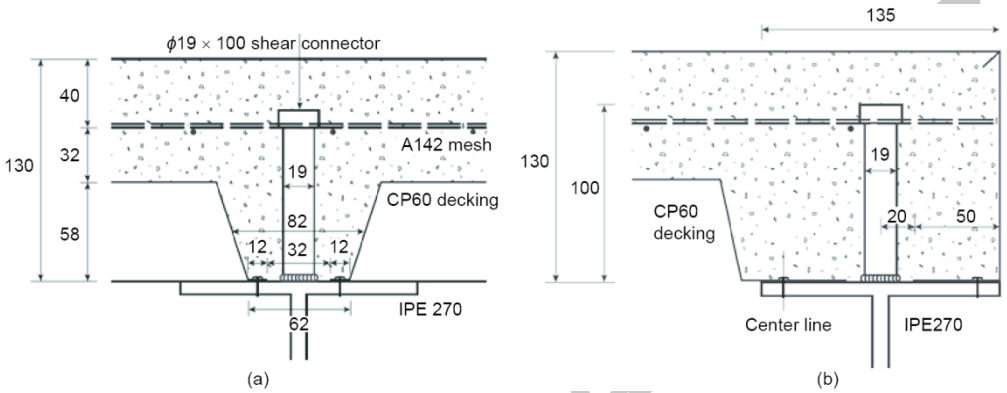

Fig. 5. Details for shear connectors at (a) the central primary beam and (b) the edge primary beam. Unit: mm.

The reinforcement adopted for the specimen was A142 mesh, as shown in Fig. 6, which was equivalent to the 0.2% minimum reinforcement in the concrete topping according to Eurocode 4. It was positioned 40 mm from the top of the slab, as shown in Fig. 5, so that it was just below the head of the shear connectors. The decking was discontinuous at the internal primary beam but continuous elsewhere. This was done so that the decking did not act as effective transverse reinforcement. To compare the effects of having no U-shaped reinforcing bar (U-bar), 10 mm U-bars were placed around the shear connectors only on one edge of the floor plate. Fig. 6(a) shows the reinforcement mesh in place and the details of the U-bars. The floor plate was cast unpropped. Fig. 6(b) shows the whole composite floor plate after casting.

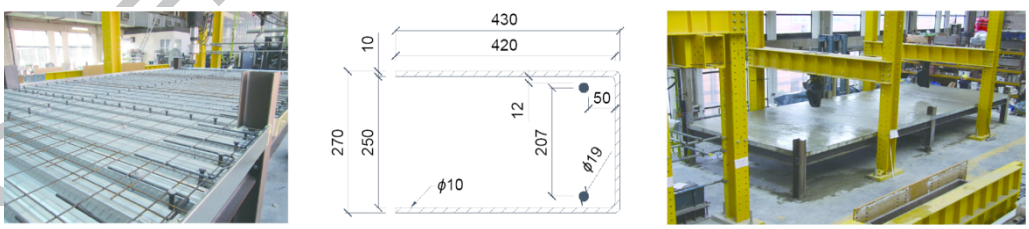

Fig. 6. Composite floor plate specimen before and after concrete casting. (a) Reinforcement mesh for the specimen; (b) the dimension of the U-bars arranged at the edge (unit: mm); (b) composite floor plate after casting.

To monitor the concrete strength development, 15 cubes with the dimensions 100 mm × 100 mm × 100 mm were cast when casting the floor plate specimen. The average concrete compressive cube strength measured at 28th day was 32.7 $N \cdot mm^{-2}$ and the average concrete compressive cube strength measured on the test date was 33.8 $N \cdot mm^{-2}$, which is consistent with the target strength of C25/30 concrete. The yield strength and ultimate strength for the steel sections were measured at 420 and 525 $N \cdot mm^{-2}$, respectively. Fig. 7 shows the stress-strain relationship of the steel material from the coupon test.

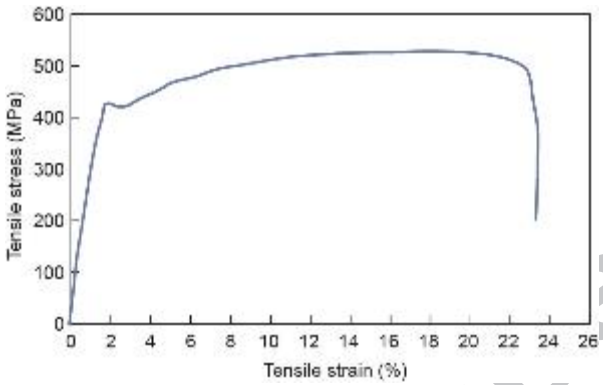

Fig. 7. Stress-strain curve of the steel material.

The shear connector resistance was calculated using the equations from EN 1994-1-1 [7] and was determined to be 61 kN for the case where the decking was perpendicular to the beam; this is consistent with the push-out tests carried out by our project partners. Fig. 8 shows the load versus slip curve from the push-off test with the same arrangement.

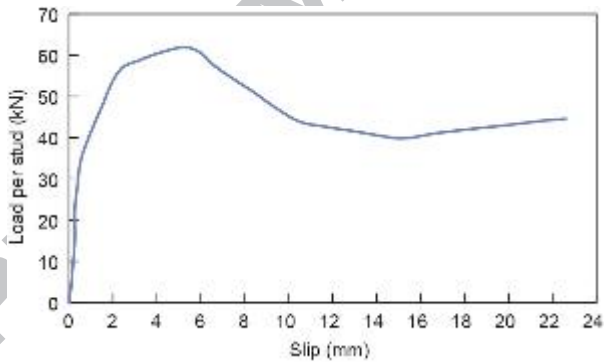

Fig. 8. Load vs. slip curve of the push-off test.

2.5. Instrumentation

To monitor the deformation and strain of the steel beams, numerous linear variable displacement transducers (LVDTs) and strain gauges were installed. Fig. 9 shows the positions of the LVDTs. Of these, LVDTs 1–9 measured the vertical displacement in the beams at mid-span and LVDTs 10–13 measured the relative slip between the concrete slab and the internal secondary beams when loading the internal secondary beams in the first test. When the actuators moved to load the edge secondary beams, LVDTs 10–13

measured the relative slip between the concrete slab and the secondary edge beams. LVDTs 15–16 monitored the horizontal deformation of the central column. Fig. 10 shows the strain gauge positions through which typical strains on the beams were recorded.

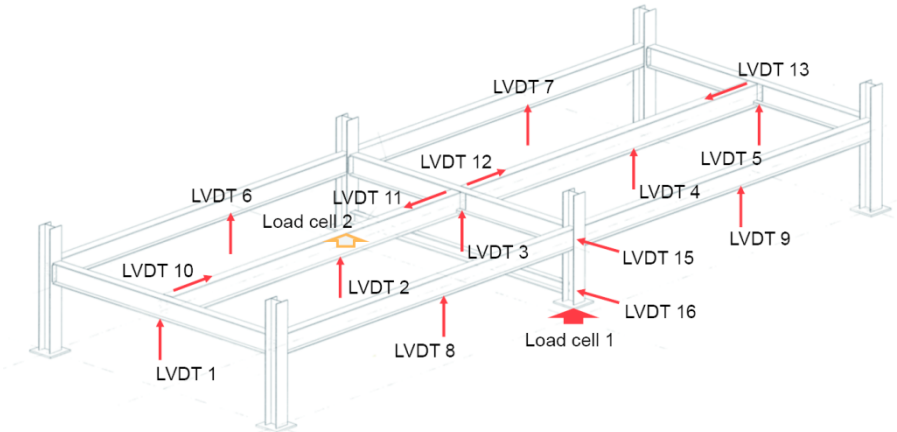

Fig. 9. Three dimentional (3D) view of the deflection monitoring positions (LVDTs 1–16).

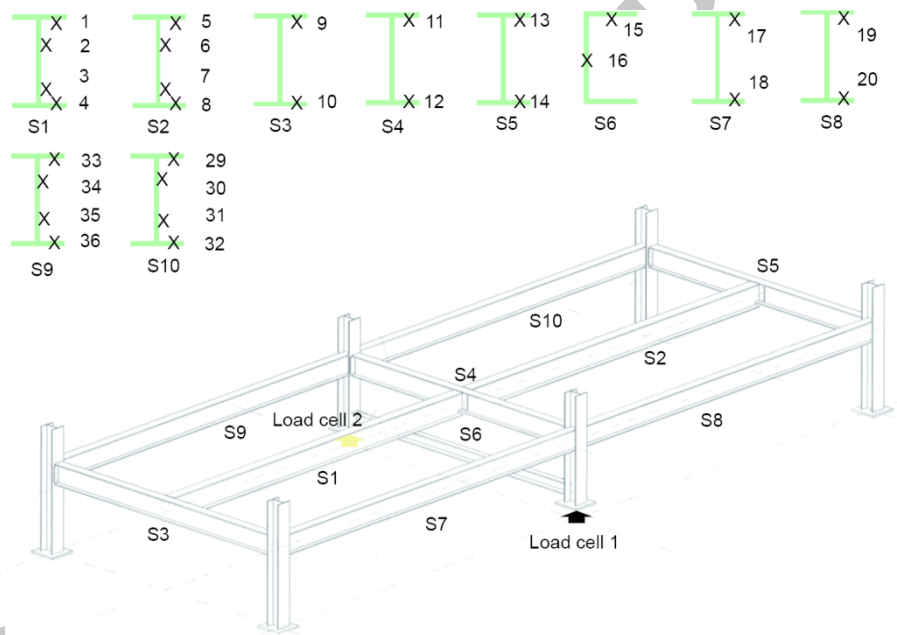

Fig. 10. 3D view of the strain-monitoring positions (S1–S10) on the steel beams: All monitoring sections are at the beam mid-span and in the axis direction.

3. Test results

3.1. Loading on primary beam through internal secondary beams

The loading of the primary beam occurred through the point loads on the internal secondary beams, as shown in Fig. 11. The load positions on the secondary beams were

placed 1.4 m apart and were placed at a distance of 1.92 m to the web of the supporting primary beams, which is equivalent to 37% of the span; this was done in order to obtain the required moment and shear distribution. For the secondary beams, there were nine shear connectors from the support (primary beam) to the loading point. For the primary beams, there were eight shear connectors from the column face to the beam mid-span (where the internal secondary beam joined the primary beam).

In total, five loading cycles were conducted. The loading by the actuators was converted to an equivalent uniform loading by dividing the load by 9.93 m^2 (5.24 m × 1.895 m). During the first four cycles of the test, the load was increased up to 20 $kN \cdot m^{-2}$ (corresponding to a point load of 99.3 kN). Next, in the fifth cycle, the load was increased to the eventual failure load of 46 $kN \cdot m^{-2}$, which corresponds to a point load of 228.4 kN. Typical deflections and strains of the beams and columns were recorded during the tests.

Fig. 11. Loads applied to the internal secondary beam.

Table 1 summarizes the maximum deflections and slips that correspond to the maximum load for each loading cycle and the residual deformation after unloading. Up to the test load of 20 $kN \cdot m^{-2}$, the maximum vertical deflection at the mid-span of the edge secondary beam (LVDT 8) was 2.17 mm; this was about 18% of the maximum vertical deflection at the mid-span of the internal secondary beam (LVDT 2), which was 11.9 mm. The maximum deflections at the mid-span of the central and edge primary beams (LVDT 3 and LVDT 1) were 5.03 and 2.45 mm, respectively. All residual deflections after unloading were very small—less than 2 mm. At the failure load of 46 $kN \cdot m^{-2}$, which corresponded to the total equivalent uniform failure load of 49 $kN \cdot m^{-2}$ including the self-weight of the slab (3 $kN \cdot m^{-2}$), the maximum deflection at the internal secondary beam (LVDT 2) was 68.3 mm. The maximum deflections for the central and edge primary beams (LVDT 3 and LVDT 1) were 22.3 and 7.14 mm, respectively. The average value of the deflection of the primary beams was 14.7 mm at the failure load, so the net deflection of the internal secondary beam at the failure load was equal to 54 mm (span/96). Fig. 12 shows the deformed shape of the secondary beams.

Table 1
Summary of deflection or slip at the maximum load for loading internal beams (unit: mm).

Load condition	Cycle 1 6 $kN \cdot m^{-2}$		Cycle 2 10 $kN \cdot m^{-2}$		Cycle 3 15 $kN \cdot m^{-2}$		Cycle 4 20 $kN \cdot m^{-2}$		Cycle 5 46 $kN \cdot m^{-2}$	
	Max	Resi.	Max	Resi.	Max	Resi.	Max	Resi.	Max	Resi.
LVDT 1	0.60	0.02	1.04	0.01	1.66	0.12	2.45	0.20	7.14	0.58
LVDT 2	2.40	0.10	4.31	0.34	7.42	0.94	11.90	1.94	68.30	29.90
LVDT 3	1.10	0.05	1.93	0.12	3.34	0.40	5.03	0.67	22.30	8.95
LVDT 4	2.10	0.04	3.90	0.28	6.78	0.91	10.90	1.88	51.40	17.40

LVDT 5	0.50	0.01	0.82	0.03	1.38	0.14	2.13	0.28	6.50	0.74
LVDT 6	0.60	0.02	0.93	0.08	1.37	0.17	2.02	0.31	—	—
LVDT 8	0.50	0.04	0.82	0.11	1.28	0.23	2.17	0.50	7.17	1.34
LVDT 9	0.60	0.03	1.03	0.06	1.63	0.14	2.34	0.22	4.96	0.68
LVDT 10	0.08	0.06	0.12	0.07	0.20	0.10	0.39	0.18	5.50	4.90
LVDT 11	0.04	0.04	0.12	0.12	0.23	0.16	0.31	0.20	—	—
LVDT 12	0.05	0.01	0.09	0.01	0.14	0.01	0.22	0.02	1.11	0.76
LVDT 13	0.04	0.02	0.06	0.03	0.12	0.05	0.22	0.09	0.07	0.12
LVDT 15	0.12	0.05	0.12	0.06	0.21	0.07	0.14	0.14	0.98	0.82
LVDT 16	0.07	0.10	0.14	0.01	0.10	0.07	0.07	0.09	0.30	0.15

In the table, "—" indicates no LVDT installed.

Fig. 12. Deflection of internal secondary beams at maximum load.

The measured deflection of the adjacent edge beams (LVDT 8) was 7.17 mm, which was approximately 13% of the net deflection of the internal secondary beam. The relative slips between the internal secondary beam and the concrete slab are summarized in Table 1. It can be seen that the slip is less than 6 mm (by LVDT 10). After all the tests were finished, no shear stud had fractured; therefore, the slip of LVDT 10 was mainly due to the cracking of the concrete slab. The horizontal deflection of the central column (by LVDT 15) was less than 1.0 mm at the failure load of 46 $kN \cdot m^{-2}$. This means that the moment applied to the column by the central primary beam to the column connection was small. Fig. 13 shows the load-versus-displacement curves.

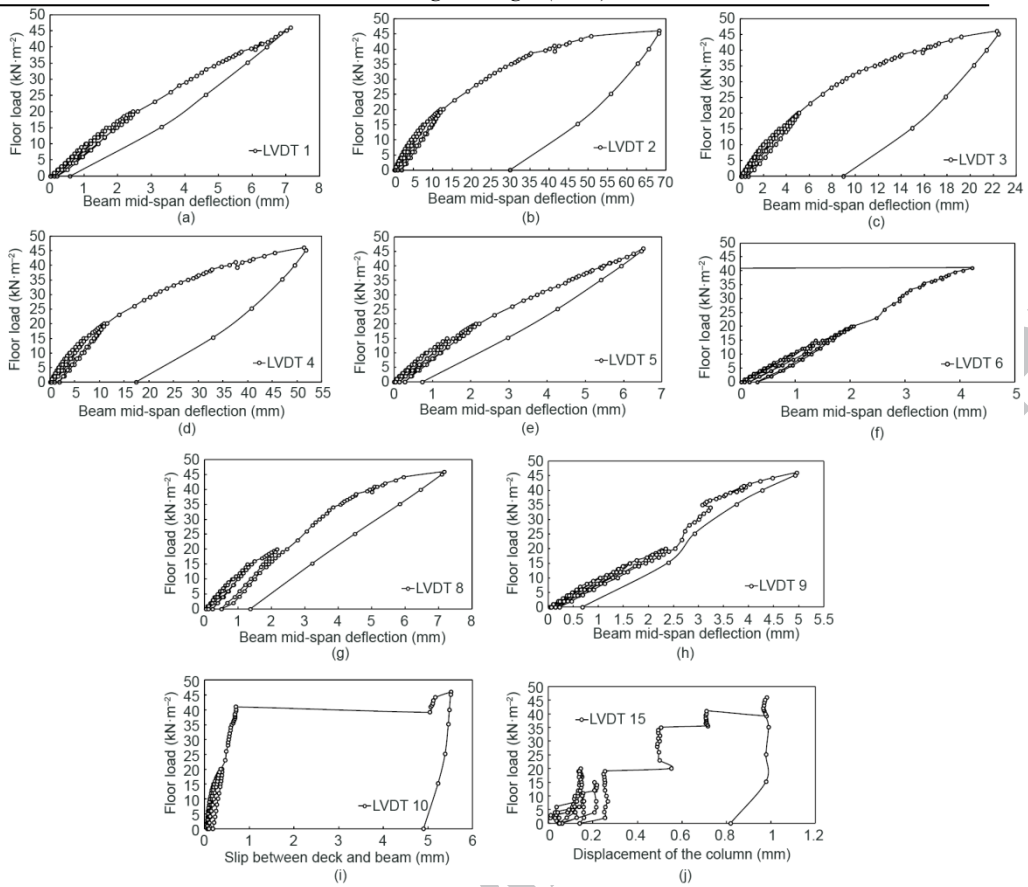

Fig. 13. Typical load-vertical displacement at beam mid-span: (a) LVDT 1; (b) LVDT 2; (c) LVDT 3; (d) LVDT 4; (e) LVDT 5; (f) LVDT 6; (g) LVDT 8; (h) LVDT 9; (i) LVDT 10; and (j) LVDT 11.

Table 2 summarizes the maximum strains at the maximum load of each loading cycle and the residual strains after unloading. Fig. 14 shows typical stress-strain developments at the mid-span of the internal secondary beams and central primary beam; it can be seen that the strain of the secondary beam was small up to a load of 20 kN·m^{-2}. At the failure load of 46 kN·m^{-2}, no strain value exceeded 2000 με in the secondary beams. The strain in the central primary beam indicated that the top flange nearly reached a compressive strain of 2000 με at a load of approximately 45.5 kN·m^{-2}. The bottom flange reached a tensile strain of 2000 με at a load of 27 kN·m^{-2}. As the horizontal movement of the lower part of the central columns was small, the strain in the linking channel beam was also very small. As shown in Table 2, the strain at the mid-span of the edge secondary beams was small; even at the failure load, no strain value reached 2000 με. The strain in the top surface of the concrete slab was also small due to the occurrence of cracks next to the strain gauges. Fig. 15 shows the cracks that developed in the slab top surface along the central primary beam. The crack width along the central primary beam was measured manually using a crack microscope and was recorded in loading cycle 5: A crack width of 0.5–0.8 mm developed at 10 kN·m^{-2}, and 1.2–1.6 mm wide cracks occurred at 20 kN·m^{-2}. The crack widths increased to 1.5–2.0 mm at 30 kN·m^{-2} and to 1.7–3.7 mm at 40 kN·m^{-2}. At the failure load of 46 kN·m^{-2}, the crack widths were around 2.7–4.7 mm.

Table 2
Summary of typical strains at the maximum load for loading internal beams (unit: με).

Load conditions		Cycle 1 6 kN·m^{-2}		Cycle 2 10 kN·m^{-2}		Cycle 3 15 kN·m^{-2}		Cycle 4 20 kN·m^{-2}		Cycle 5 46 kN·m^{-2}	
		Max	Resi.	Max	Resi.	Max	Resi.	Max	Resi.	Max	Resi.
S1	S1-1	/	/	/	/	/	/	/	/	–1256	–458
	S1-3	/	/	/	/	301	27	431	51	1918	836
	S1-4	/	/	258	21	416	42	629	88	1578	–157
S2	S2-5	/	/	/	/	/	/	/	/	–961	–358
	S2-7	/	/	/	/	288	19	406	34	1325	336
	S2-8	/	/	242	/	394	36	582	66	1837	–89
S3	S3-9	/	/	/	/	/	/	−256	−84	–1008	–152
	S3-10	/	/	/	/	301	35	445	60	1352	289
S4	S4-11	/	/	/	/	/	/	−212	−116	–2331	–1513
	S4-12	253	506	444	/	713	32	1043	46	> 10000	Failed
S5	S5-13	/	/	/	/	/	/	/	/	–718	–24
	S5-14	/	/	/	/	259	26	374	43	1231	258
S7	S7-18	/	/	/	/	/	/	/	/	396	96
S8	S8-20	/	/	/	/	/	/	/	/	367	88

" / " indicates a small value with a maximun strain less than 200 με or a residual strain less than 20 με. All the maximun strains recorded at stain gauge positions S1-2, S2-6, S6-15, S6-16, S7-17, and S8-19 were less than 200 με and are therefore not shown in the table.

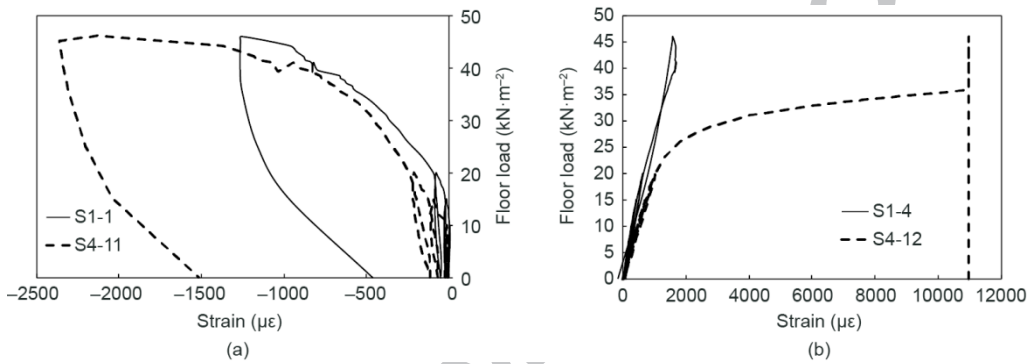

Fig. 14. Typical stress-strain curves of the steel beam for the strain-monitoring positions of (a) S1-1/S4-11 and (b) S1-4/S4-12.

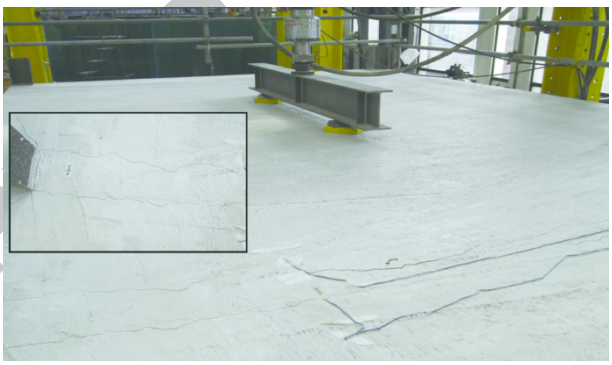

Fig. 15. Cracks at the top surface of the slab along the central primary beam.

Based on the deflections recorded in the secondary and primary beams, it can be seen that the load applied to the internal secondary beams was mainly transmitted to the primary beams, and only a small proportion of the load was transmitted to the secondary edge beams through the concrete slab due to the flexure of the floor slab. A calculation of the bending resistance of the internal secondary beam according to Eurocode 4, assuming a shear connector resistance of 61 kN per stud, determined that the equivalent uniform

load was 38 kN·m^{-2} plus the self-weight of the slab and load frame (3.3 kN·m^{-2}). This is equivalent to 82% of the actual test load of 46 kN·m^{-2}, plus the self-weight of the slab and load frame (3.3 kN·m^{-2}). Therefore, it appears that about 80% of the applied load was transmitted to the primary beams through the internal secondary beams. The remaining load was transferred via the edge beams to the columns due to flexure of the floor slab through the edge secondary beams. The connections to the primary beams did not transmit any moment.

3.2. Tests on edge beams with and without the U-bars

The loading on each of the edge secondary beams was applied directly to the beam by two point loads, as shown in Fig. 16. To calculate the loaded area acting on the edge beam, the loaded width of the slab was calculated based on half of the spacing between the center line of the secondary beams (= 1.89 m /2) plus the slab edge distance of 0.1 m. The load applied by the actuator was converted to an equivalent uniform loading by dividing the load by 5.5 m^2 (given the loaded area of 5.24 m × 1.05 m = 5.5 m^2). In total, three loading cycles were performed on each edge beam. The first two cycles of loading were applied up to 40 kN·m^{-2}. The load in the third cycle was then increased to the eventual failure load of 60 kN·m^{-2}. Typical deflections and strains of the beams and column were recorded. The displacement transducer and typical strain gauge positions are shown in Figs. 9 and 10. Table 3 summarizes the maximum deflection and slip at the maximum load of each cycle and the residual deformation after unloading. Table 4 summarizes the typical maximum strains that occurred at the maximum load of each cycle and the residual strains after unloading. Fig. 17 presents typical load-deflection relationships at typical monitoring positions. Fig. 18 shows typical strain observations.

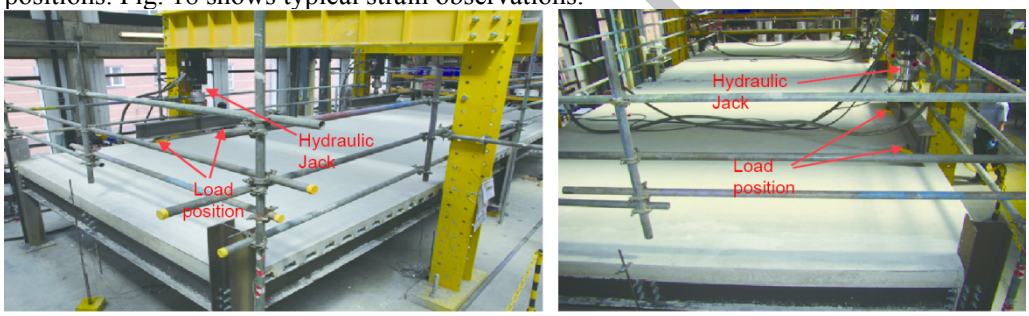

Fig. 16. Edge beam tests (a) with and (b) without U-bars.

Table 3
Summary of deflection or slip at the maximum load for loading edge beams (unit: mm).

Load condition	Test on edge beam without U-bars						Test on edge beams with U-bars					
	Cycle 1 30 kN·m^{-2}		Cycle 2 40 kN·m^{-2}		Cycle 3 60 kN·m^{-2}		Cycle 1 20 kN·m^{-2}		Cycle 2 40 kN·m^{-2}		Cycle 3 63 kN·m^{-2}	
	Max	Resi.	Max	Resi.	Max	Resi.	Max	Resi.	Max	Resi.	Max	Resi.
LVDT 1	0.25	0.09	0.35	0.01	0.57	0.11	0.34	0.03	0.59	0.06	1.06	0.38
LVDT 2	1.97	0.55	2.88	0.01	5.56	0.26	1.20	0.09	2.67	0.27	5.77	0.95
LVDT 3	0.53	0.26	0.83	0.01	1.92	0.03	0.43	0.07	1.13	0.09	2.31	0.32
LVDT 4	1.81	0.57	2.55	0.01	5.18	0.07	1.30	0.04	2.80	0.01	5.18	0.24
LVDT 5	0.17	0.09	0.27	0.01	0.72	0.10	0.20	0.03	0.47	0.07	0.80	0.19
LVDT 6	0.57	0.01	0.74	0.03	0.97	0.22	7.38	0.50	20.00	2.81	74.20	36.90
LVDT 7	—	—	—	—	—	—	7.24	0.70	19.20	2.94	50.30	17.90
LVDT 8	14.40	1.92	23.20	3.88	69.30	29.70	—	—	—	—	—	—
LVDT 9	12.50	1.84	20.60	3.70	48.70	16.00	—	—	—	—	—	—
LVDT 10	0.09	0.03	0.16	0.04	0.16	0.03	0.06	0.01	0.15	0.07	0.61	0.30
LVDT 11	0.10	0.04	0.01	0.04	0.92	0.19	0.09	0	0.04	—	—	—
LVDT 12	0.11	0.02	0.21	0.02	0.80	0.22	0.09	0.01	0.35	0.04	0.46	0.05

LVDT 13	0.11	0.03	0.02	0.04	0.29	0.16	0.09	0.01	0.16	0.01	0.11	0.02

In the table, "—" indicates no LVDT installed.

Table 4
Summary of typical strains at the maximum load for loading edge beams (unit: με).

		Cycle 1 (30 kN·m^{-2})		Cycle 2 (40 kN·m^{-2})		Cycle 3 (60 kN·m^{-2})	
		Max	Resi.	Max	Resi.	Max	Resi.
Load on edge beam without U-bars							
S7	S7-17	–242	–57	–514	–130	–1525	–377
	S7-27	31	/	–73	–58	–261	90
	S7-28	559	50	802	102	3198	1949
	S7-18	872	89	1302	184	2286	243
S8	S8-19	–127	–31	–325	–81	–885	–188
	S8-25	91	/	21	–39	–127	/
	S8-26	558	51	781	89	1719	544
	S8-20	790	76	1165	142	2122	307
		Cycle 1 (20 kN·m^{-2})		Cycle 2 (40 kN·m^{-2})		Cycle 3 (63 kN·m^{-2})	
		Max	Resi.	Max	Resi.	Max	Resi.
Load on edge beam with U-bars							
S9	S9-33	–98	/	–437	–102	–1522	–373
	S9-34	69	/	17	–29	–150	125
	S9-35	343	/	779	86	2537	1358
	S9-36	477	/	1159	144	7809	5816
S10	S10-29	–63	/	–313	–74	–968	–237
	S10-30	67	/	40	–47	–24	38
	S10-31	343	/	753	83	1810	642
	S10-32	455	/	1056	109	2287	516

" / " indicates a small value or a maximum strain less than 50 με and a residual strain less than 30 με.

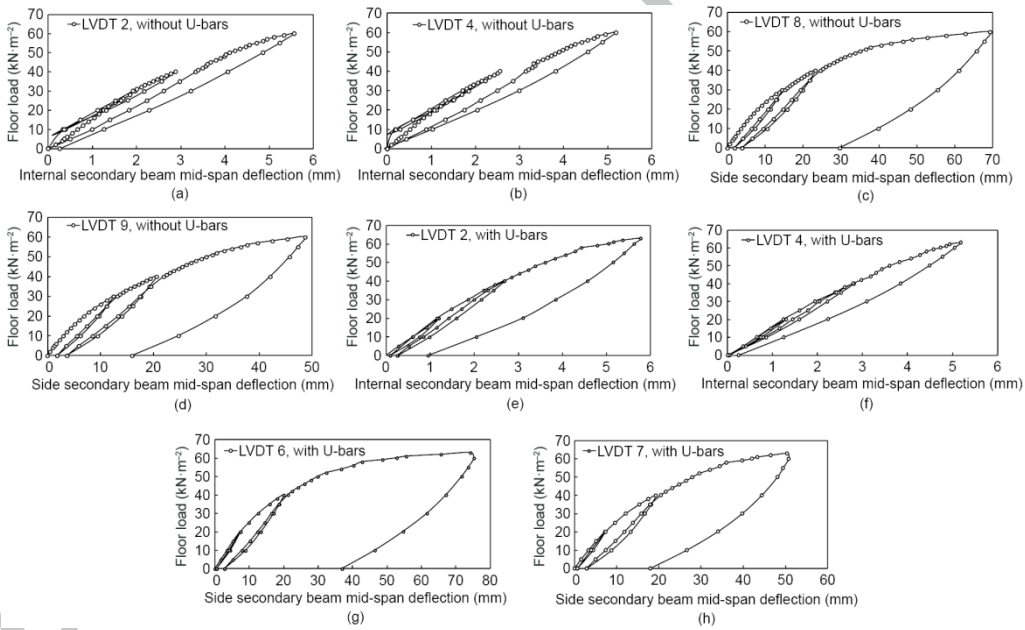

Fig. 17. Graphs for load-deflection at beam mid-span. Tests on edge beams (a–d) without and (e–h) with the U-bars.

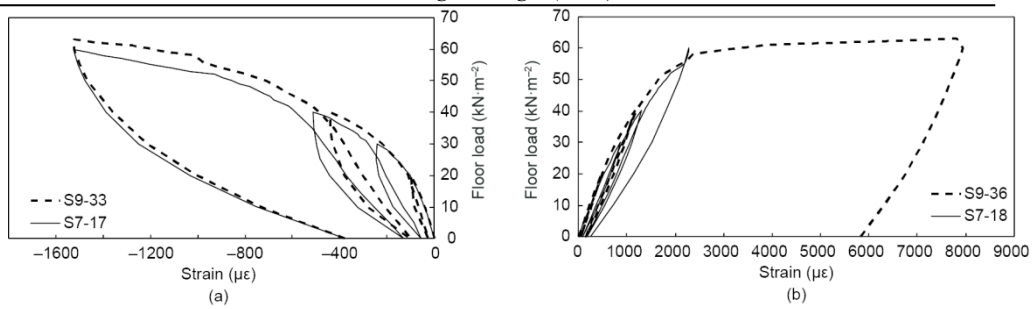

Fig. 18. Typical stress-strain graphs for (a) S7-11/S9-33 and (b) S7-18/S9-36 for loading through the edge beam.

From Fig. 18 and Table 4, it can be seen that the tensile strain in the beam lower flange and web were over 2000 με (S7-18, S7-28, and S8-20) for the edge beam without U-bars when the loading were applied up to 60 kN·m^{-2}. In addition, for the edge beam with U-bars, the strain at the beam mid-span exceeded 2000 με (S9-35, S9-36, and S10-32) before the load reached the failure load. The strain distribution clearly indicates that the neutral axis of the composite beam was in the web above the central line when the load increased to 40 kN·m^{-2}.

According to the test observations, given the typical displacements summarized in Table 3 and shown in Fig. 17, it is apparent that the loaded secondary edge beam behavior was still essentially elastic up to an equivalent uniform loading of 30 kN·m^{-2}. The failure load occurred at an equivalent uniform loading of 60 kN·m^{-2} for the edge beam without U-bars and 63 kN·m^{-2} for the edge beam with U-bars; the latter is about 5% higher than that of the beam without U-bars. It is apparent that the composite beam with U-bars is slightly stiffer than the composite beam without U-bars (comparing a deflection of 23.2 mm (LVDT 8, without U-bars) and 20 mm (LVDT 6, with U-bars) at an equivalent loading of 40 kN·m^{-2}). This is probably due to a lower level of cracking that was observed in this case, which reduced the longitudinal slip. In addition, the residual deflection on unloading from 40 kN·m^{-2} was 2.81 mm for the beam with U-bars (LVDT 6) in comparison with 3.88 mm (LVDT 8) for the beam without U-bars. According to the test observation, for the edge beam without U-bars, the maximum mid-span deflection of the loaded secondary edge beam was 69.3 mm (LVDT 8) with a residual deflection of 29.7 mm on unloading. The mid-span deflections of the internal secondary beams were small, at 5.56 mm (LVDT 2) and 5.18 mm (LVDT 4), respectively, which is about 8% of the loaded edge beam deflection. It is estimated that about 10% of the applied load acting on the loaded edge beams was transferred to the internal secondary beams via the transverse stiffness of the concrete slab. From Table 3, it can be seen that the slip between the slab and the secondary edge beam was less than 1 mm (LVDTs 10–13), even at the failure loads. The deflections at the mid-span of the central primary beam (LVDT 3) were 2.31 mm and 1.92 mm at the failure loads for beams with and without U-bars, respectively. The maximum mid-span deflection of the edge primary beam was less than 1.1 mm (LVDTs 1 and 5).

Fig. 19 clearly shows the cracking pattern due to the longitudinal shear failure for the edge beam without U-bars and the edge beam with U-bars at failure. For the secondary edge beam with U-bars, the shear connector resistance was assumed to be fully developed and was taken as 61 kN per stud. Given the effective width of the compression flange of the edge beam of b_{eff} = 100 + 5240/8 = 755 mm, concrete cylinder strength of 27 N·mm^{-2},

steel yield strength of 420 N·mm^{-2}, stud central spacing of 207 mm, and nine shear connectors between the support and the point load position, a calculation of the bending resistance of the secondary edge beam according to Eurocode 4 showed that the applied load of 314 kN corresponded to an equivalent uniform load of 57 kN·m^{-2}. This is about 91% of the actual test load of 63 kN·m^{-2}. For the edge beam without U-bars, the shear connector resistance reduction factor was calculated by $k_{t,edge} = 0.5(1 + e/(8\phi))$. By setting e = 100 mm and ϕ = 19 mm, and then $k_{t,edge}$ = 0.83, the shear connector resistance was determined to be 61 × 0.83 = 50.6 kN per stud. The calculated bending resistance of the secondary edge beam without U-bars according to Eurocode 4 was 298 kN, which corresponded with the equivalent uniform load of 54 kN·m^{-2}; this was about 91% of the actual test load of 60 kN·m^{-2}. Both the calculation and test results showed that about 5% reduction of moment resistance due to the omission of the U-bars.

(a) (b)

Fig. 19. (a) Crack at the edge of the slab without U-bars at failure, and (b) deflection of the edge beam with U-bars.

3.3. Tests on column removal

A pseudo-robustness test was performed by removing the support under a central edge column, which had been detailed to be 200 mm shorter than the others in order to install the load cell. Therefore, the deflection of the column could be measured upon removal of the support while being subjected to additional loads from the beams. For practical reasons, the edge beams were loaded rather than the column itself, although this would cause the same effect of adding to the deflection of the columns and further deforming the edge beams, which were severely damaged by the previous tests. Fig. 20 shows the displacement transducers' position. LVDTs 8 and 9 measured the vertical displacement of the edge beam at mid-span, LVDTs 15 and 16 measured the horizontal displacements of the column, and LVDTs 17–20 monitored the column's vertical displacement.

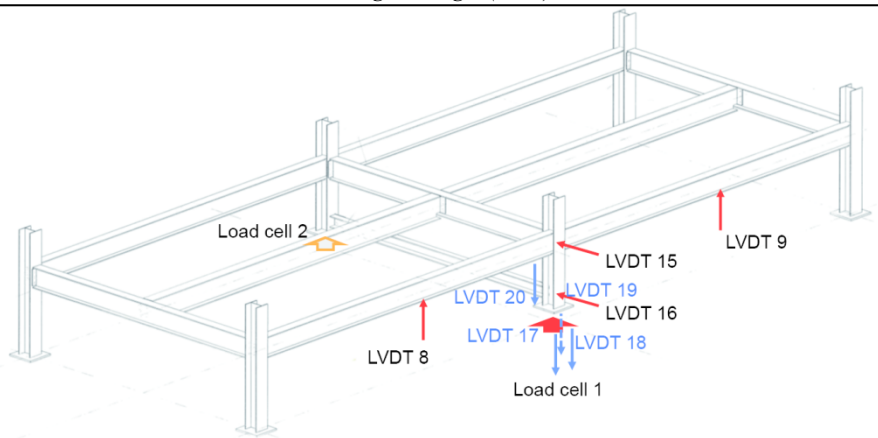

Fig. 20. 3D view of the deflection measurement positions.

The measured deflection of the central edge column upon removal of its support was 36 mm when subjected to a load of 3 kN·m^{-2}, due to the self-weight of the slab and beams (as shown in Fig. 20, where no load was imposed from the actuator). The equivalent load acting on the missing column was 33 kN due to the self-weight. The deflection corresponded to an inclination of 1 in 145 for the edge beam, which was small.

The load was applied at the mid-span of the edge beams and was presented as an equivalent uniform loading acting on the floor slab. The point load acting on each beam was divided by an area of 5.5 m^2 in order to obtain the equivalent uniform loading, as shown in Fig. 21.

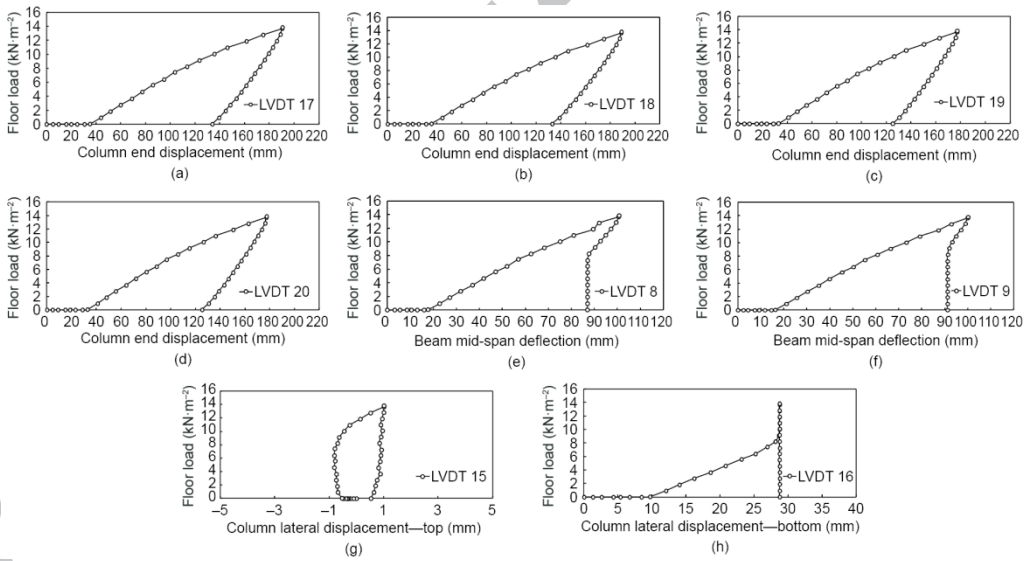

Fig. 21. Measured displacements.

The maximum displacement of 190 mm was reached for an equivalent uniform loading of 13.8 kN·m^{-2} in addition to the self-weight (Fig. 21, LVDTs 17–20), which corresponded to a point load of 75 kN per actuator acting on each beam. This also corresponded to a notional load of 75 kN acting on the central edge column with its

missing support. The maximum displacement corresponded to an inclination of 1 in 27 or about 2 degrees for the edge beam. The vertical displacement at the mid-span of the edge beams was about 100 mm (LVDTs 8 and 9). No significant horizontal sway was observed from the missing column, as recorded by LVDTs 15 and 16. It is apparent that the maximum load capacity of the floor system had not been reached at the maximum displacement of 190 mm, and a further increase of 20% to 30% in loading might have been possible. This would correspond to a missing column load of 133 kN. The deflected shape of the floor plate at the end of the test is shown in Fig. 22.

The maximum strain recorded in the flanges of the edge beams at the mid-span was around 1000 με, and that at the monitoring sections close to the column was about 1800 με. The strains in the primary beam were small. This indicates a tensile stress of 39 $N \cdot mm^{-2}$ in the cross-section and a tension force of 179 kN. The total applied load on the missing column was 33 + 75 = 108 kN. For an edge beam with inclination of 1 in 27, this indicates a catenary force in the edge beams of 1458 kN. Thus, the catenary action in the test was about 12% of the maximum value, with the remaining resistance being provided by the membrane forces in the slab.

Fig. 22. Deflection of the edge beam due to missing support to the central column.

4. Conclusions

According to the test observations and results, the following conclusions can be made from the floor plate tests:

- From the internal beam tests, it was estimated that the internal secondary and primary beams resisted 80% of the applied floor load, while 20% of the applied load was transferred by the secondary edge beams due to the transverse stiffness of the slabs.
- The central primary beam was found to be stronger than the plastic bending resistance despite having slightly less transverse reinforcement than required by Eurocode 4. The failure load was 14% higher than that calculated using a shear connector resistance of 61 kN. The internal secondary beams failed at an equivalent uniform loading of 49 $kN \cdot m^{-2}$ (including the self-weight of the slab), which when reduced by 20% as noted above, gave a moment of 95% of the plastic bending resistance calculated using the Eurocode 4 method.
- From the edge beam tests, the edge beam with U-bars around the shear connectors failed at an equivalent uniform loading of 66 $kN \cdot m^{-2}$ (including the self-weight of the slab), and the beam without U-bars failed at an equivalent uniform loading of 63 $kN \cdot m^{-2}$ (5% less). Considering a 10% transfer of load from the edge secondary beam to the internal secondary beam, the edge secondary beams failed at a moment that was very close to the calculated plastic bending resistance.

- In terms of deflections, it was apparent from the tests on the internal secondary beams that the effects of slip on deflections were less than calculated for a load level up to 10 $kN \cdot m^{-2}$. This is due to the continuity effects of the mesh reinforcement in the slab. The measured deflection of the primary beam was higher than calculated for a load level of 20 $kN \cdot m^{-2}$, which shows that the effect of stiffness of the connections to the columns was relatively small.
- For the edge beams that were subject to an equivalent uniform loading of 20 $kN \cdot m^{-2}$, the measured deflections were 7.4 mm with U-bars and 8 mm without U-bars, compared with a theoretical deflection of 6.2 mm including the effects of slip. This shows that for edge beams, the effects of slip are greater for higher load levels. The comparisons were very close for lower load levels. The effect of the lack of U-bars was relatively small.
- It is concluded that the floor structure can resist an equivalent load of 108 kN with the missing column scenario, which when divided by the supported floor area of 10.5 m^2, corresponds to a floor loading of about 10 $kN \cdot m^{-2}$, including the slab self-weight. This finding demonstrates the robustness of composite floors after the removal of a column.

Acknowledgements

The research covered in this paper is part of a collaborative project between the Steel Construction Institute, the University of Stuttgart, the University of Luxembourg, Arcelor Mittal S.A., and the University of Bradford, and was funded by the European Community's Research Fund for Coal and Steel under grant agreement (RFSR-CT-2012-00030).

Compliance with ethics guidelines

Dennis Lam, Xianghe Dai, and Therese Sheehan declare that they have no conflict of interest or financial conflicts to disclose.

References

[1] Bailey CG. Membrane action of slab/beam composite floor systems in fire. Eng Struct 2004;26(12):1691–703.
[2] Lam D, Elliott KS, Nethercot DA. Designing composite steel beams with precast concrete hollow-core slabs. Proc Inst Civil Engs—Struct Build 2000;140(2):139–49.
[3] Ellobody E, Young B. Performance of shear connection in composite beams with profiled steelsheeting. J Constr Steel Res 2006;62(7):682–94.
[4] Sheehan T, Dai X, Lam D, Aggelopoulos E, Lawson M, Obiala R. Experimental study on long spanning composite cellular beam under flexure and shear. J Constr Steel Res 2016;116:40–54.
[5] Ranzi G, Bradford MA, Uy B. A general method of analysis of composite beams with partial interaction. Steel Compos Struct 2003;3(3):169–84..
[6] Yang Y, Yu Y, Zhou X, Roeder CW, Huo X. Study on mechanical performance of composite beam with innovative composite slabs. Steel Compos Struct 2016;21(3):537–51.
[7] EN 1994-1-1: Eurocode 4—Design of composite steel and concrete structures—Part 1-1: General rules and rules for buildings. European standard. Brussels: European Committee for Standardization; 2004.